Bulgarian Chemical Communications, Volume 58, Issue 4 (pp. 482-491) 2026 *DOI: 10.34049/bcc.58.4.5753*

Fitting and interpretation of equilibrium and kinetic models, and two-stage adsorber design of condensate-based adsorbents for methylene blue removal

T. F. Rahaman [1,2], F. Amran[1,2], M. A. A. Zaini[1,2*]

[1] *Faculty of Chemical & Energy Engineering, Universiti Teknologi Malaysia, 81310 UTM Johor Bahru, Johor, Malaysia*

[2] *Centre of Lipids Engineering and Applied Research (CLEAR), Ibnu-Sina Institute for Scientific and Industrial Research, Universiti Teknologi Malaysia, 81310 UTM Johor Bahru, Johor, Malaysia*

Received: February 13, 2026; Revised: June 17, 2026

The present work aims at evaluating the equilibrium and kinetic models, and traits of a two-stage adsorber in optimizing the mass of condensate-based adsorbents for methylene blue removal. Results show that CZ1.5 and CS0.5Z recorded high methylene blue capacities of 191 and 193 mg/g, respectively. The adsorption data obeyed the Langmuir model, while the kinetic data closely fitted a pseudo-second order model. In a two-stage adsorber design, to improve the removal efficiency from 80 % to 99 %, the total adsorbent mass has to be increased by 94.2 % due to strong liquid-phase mass transfer resistance and weak adsorbate-adsorbent affinity. Nonetheless, the mass required can be reduced by 54.8 % for treating any volumes of dye effluent. In the performance evaluation, the mass in stage-1 is higher than that in stage-2 for lessening the surface load to achieve equilibrium at minimum dosage. The two-stage adsorber aids to optimize the mass for different percentages of dye removal that are economically feasible for industrial applications.

Keywords: Palm oil condensate, adsorption, environmental engineering, methylene blue, wastewater treatment

INTRODUCTION

Textile printing and dyeing industry plays a vital role in modern society and is experiencing rapid advancement. The industry uses a large amount of water during wet processing and leads to a significant increase in the volume of wastewater heavily laden with dissolved dyes. The industry consumes around 1.6 million liters of water each day to produce approximately 8,000 kg of fabric [1]. There are more than 10,000 different dyes used in textile manufacturing, with nearly 70 % comprising azo dyes, which are synthetic and structurally complex [2]. Dyes are highly toxic, stable, highly visible in trace amounts, and not easily biodegradable [3]. Thus, the improper discharge of dye-containing wastewater without adequate treatment poses a significant threat, particularly to environment and aquatic ecosystems. During environmental migration, dyes may react with other substances, leading to the formation of hazardous compounds [4]. The compounds can cause teratogenic and neurotoxic effects in people who consume agricultural or aquatic products contaminated by them. Also, dye-containing wastewater can hinder sunlight penetration into water bodies, thereby interfering with the photosynthesis activity of aquatic plants [5]. Therefore, it is essential to eliminate the harmful dyes from wastewater prior to its discharge into the environment.

Several treatment methods have been employed for dye removal from wastewater, including coagulation/flocculation, precipitation, membrane filtration, reverse osmosis, ozonation, advanced oxidation processes, ion exchange and adsorption [6]. Adsorption remains one of the most effective methods, offering a simple procedure using abundant and low-cost adsorbents such as activated carbon [7], biochar [8], clays [9] and zeolites [10]. Activated carbon adsorption has proven to be able to achieve high removal efficiency of dye pollutants in many scientific publications [11, 12]. Activated carbon endows a large surface area, well-developed porous texture, and rich surface functional groups to improve interaction probabilities with dye molecules in water, thus enhancing the uptake capacity [13]. The physicochemical properties of activated carbon are highly dependent on the nature of the precursor used. The precursor should be a carbon-rich material that is locally available, abundant, and economically feasible.

Palm oil condensate is a liquid byproduct produced during the processing of oil palm fruits, which can be exploited as carbon feedstock. Not all of the steam is consumed in heating the fresh fruit bunch in palm oil processing, since about half of the steam might be lost as condensate and end up as palm oil mill effluent [14]. Malaysia ranks as the world's second-largest producer of palm oil, contributing significantly to global supply. Parveez

* To whom all correspondence should be sent:
Email: *abbas@cheme.utm.my*

© 2026 Bulgarian Academy of Sciences, Union of Chemists in Bulgaria

et al. [15] reported that the rise in Malaysia's palm oil production in 2023 is attributed to a 1.9 % increase in fresh fruit bunch yield per hectare and a 0.8 % improvement in the oil extraction rate. The sustainable palm oil industry has triggered quest to capitalize the condensate as activated carbon feedstock for wastewater treatment. Chemical activation is commonly used to convert precursor into activated carbon with highly developed pore structure, resulting in enhanced dye removal capacity [16].

The single-stage batch adsorber is widely recognized as a standard approach in adsorption research. However, it is inadequate for predicting high removal efficiency under optimal adsorbent dosage and contact time conditions when scaling up the process. Hence, a two-stage adsorber design has been proposed to reduce the adsorbent mass and contact time, making the dye adsorption process more cost-effective. A 14 % reduction in adsorbent mass is achieved through the use of a two-stage adsorber employing coffee residue-based activated carbon for phenol removal [17]. In a related work, the mass for malachite green adsorption is reduced by 44 % in a two-stage adsorber of date stone activated carbon [18]. This study uniquely integrates equilibrium and kinetic model interpretations with a two-stage adsorber design for methylene blue removal using condensate-based adsorbents. The novelty of this work lies in translating the adsorption behavior into a two-stage adsorption system to optimize the mass of activated carbon. The performance evaluation was discussed to broaden the knowledge towards sustainable industrial applications.

MATERIALS AND METHODS

Palm oil condensate was collected from palm oil milling in Johor state of Malaysia. Sulfuric acid (H_2SO_4) was purchased from R&M Chemicals. Zinc chloride ($ZnCl_2$) and potassium hydroxide (KOH) were purchased from Quality Reagent Chemicals (QReC), phosphoric acid (H_3PO_4) from JT Baker. Methylene blue (MW=319.85 g/mol) was supplied by HmBG Chemicals.

Preparation and characterization of adsorbents

A 1000 mL of palm oil condensate was oven-dried for two days until its volume was reduced to 800 mL. A 400 mL of the condensate was mixed with 200 mL of H_2SO_4 solution in a 0.5 ratio (v/v, H_2SO_4: palm oil condensate). Next, pyrolysis was performed in a muffle furnace at 400 °C for 2 h. The resultant sample was designated as CS0.5. Then, it was impregnated with $ZnCl_2$ solution at a ratio of 1 (w/w, $ZnCl_2$: CS0.5). The activation was conducted in a muffle furnace at 600 °C for 1 h. The adsorbent was refluxed with distilled water in a Soxhlet apparatus for 24 h to a constant pH. The same procedures were repeated for activation by KOH. The activated carbons were designated as CS0.5Z and CS0.5K, respectively.

The adsorbents were also prepared using dried palm oil condensate with different activators. The dried condensate or sludge was impregnated with H_3PO_4 solution in a 1.5 ratio (w/w, H_3PO_4: palm oil condensate). The activation was performed in a muffle furnace at 600 °C for 1.5 h. The same procedures were repeated for activation by $ZnCl_2$. The resultant materials, designated as CH1.5 and CZ1.5 were washed with distilled water to remove impurities and oven-dried prior to use. The condensate char, labelled as CC was prepared at the same temperature and holding time, but without activator for comparison.

The CZ1.5 was characterized for surface area and pore volume nitrogen adsorption at 77 K using Micromeritics ASAP 2020. The functional groups present on the adsorbent surface were identified using a FTIR spectrometer (Thermo Scientific, Nicolet iS10). The morphological surface structure was captured using a field emission scanning electron microscope.

Batch adsorption studies

A 20 mg portion of adsorbent was added into 20 mL of methylene blue solution at concentrations ranging from 10 to 350 mg/L. The adsorbent dose was fixed at 1 mg/mL to minimize volumetric variation that could nullify the mass balance assumption. The concentrations were selected to allow surface saturation of adsorbent at equilibrium. The mixture was left to equilibrate at room temperature of 27 °C for 72 h. The contact time of 72 h was judged from the kinetic data and considering the time taken to reach equilibrium if higher dye concentrations were used. The control solution was prepared to represent the initial concentration. The concentration of methylene blue was measured using a UV-vis spectrophotometer (DU-8200) at a wavelength of 620 nm. The capacity at equilibrium, q_e (mg/g) was calculated as

$$q_e = \frac{(C_o - C_e)V}{m} \quad (1)$$

where C_o (mg/L) is the initial dye concentration, C_e (mg/L) is the equilibrium dye concentration, V (L) is the solution volume and m (g) is the adsorbent mass. The adsorption data were analyzed using Langmuir,

Freundlich and Redlich-Peterson models, as expressed in equations (2), (3) and (4), respectively,

$$q_e = \frac{q_m K_L C_e}{1+K_L C_e} \quad (2)$$

$$q_e = K_f C_e^{\frac{1}{n}} \quad (3)$$

$$q_e = \frac{K_R C_e}{1+\alpha C_e^{\beta}} \quad (4)$$

where, q_m (mg/g) is the maximum capacity, K_L (L/mg) is the Langmuir constant, K_f and n are the Freundlich constants, and K_R and α are the Redlich-Peterson constants and β is an exponent that lies between 0 and 1.

Adsorbent (20 mg) was added into 20 mL of methylene blue solution at concentrations of 7.89 and 27.5 mg/L. The mixture was allowed to reach equilibrium at room temperature of 27 °C. Kinetics is often carried out at low initial concentrations to minimize concentration-dependent mass transfer limitations and to more clearly resolve intrinsic adsorption rate behavior without saturation effects. The concentration of methylene blue was measured at different time intervals. The adsorption capacity at any time, q_t (mg/g) was calculated as

$$q_t = \frac{(C_0 - C_t)V}{m} \quad (5)$$

where C_t (mg/L) is the dye concentration at time t. The kinetic data were analyzed using pseudo-first order, pseudo-second order and intraparticle diffusion models, as expressed in equations (6), (7) and (8), respectively:

$$q_t = q_e(1 - e^{-k_1 t}) \quad (6)$$

$$q_t = \frac{k_2 q_e^2 t}{1+k_2 q_e t} \quad (7)$$

$$q_t = k_d t^{\frac{1}{2}} + C \quad (8)$$

where t (h) is the contact time, k_1 (h^{-1}) is the pseudo-first order rate constant, k_2 (g/mg.h) is the pseudo-second order rate constant, k_d (mg/g.h) is the intraparticle diffusion rate constant, and C is the intercept of the intraparticle diffusion plot.

The selection of equilibrium and kinetic models was based on their established applicability in describing dye adsorption systems and to provide complementary insights into adsorption mechanisms. The Langmuir model, for example, assumes monolayer coverage onto a homogeneous surface, while the Freundlich model accounts for multilayer stacking over heterogeneous surface. The Redlich-Peterson presents the combined features of Langmuir and Freundlich models. In addition, kinetic models were employed to evaluate the adsorption rate and potential rate-controlling steps.

Two-stage adsorption

Adsorption data were used to model the two-stage adsorber. The simulation was performed using Microsoft Excel. Figure 1 visualizes the scheme of two-stage batch adsorber design. In a two-stage adsorber, the effluent volume V first passes through stage 1, where the adsorbent mass m_1 brings the system to equilibrium at concentration C_1. The partially treated effluent then flows into stage 2, where the additional mass m_2 further reduces the concentration to a final equilibrium concentration C_2. Fresh adsorbent is supplied to each stage to treat the same volume of dye solution, resulting in adsorption capacities q_1 and q_2, respectively. The initial adsorption capacity entering each stage q_o (mg/g) = 0. The overall process can be represented by mass balance as follows:

$$V(C_0 - C_1) = m_1(q_1 - q_0) \quad (9)$$

$$V(C_1 - C_2) = m_2(q_2 - q_0) \quad (10)$$

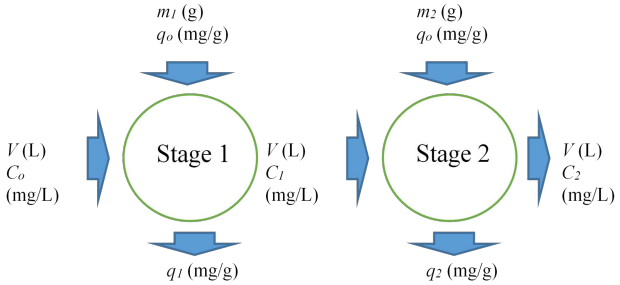

Figure 1. Two-stage adsorber design [19].

The design objective was to treat 100 mL of methylene blue solution at initial concentration C_o = 50 mg/L. A series of sorption system numbers for C_1 from 50 to 1.34 mg/L in a 2.5 mg/L step-size was considered [20]. For example, in sorption system number 1, the C_0 was reduced from 50 to 47.5 mg/L in stage-1. Similarly, in sorption system numbers 2, 3, and so on, the concentration values were reduced from 47.5 to 45.0 mg/L, 45.0 to 42.5 mg/L, and lastly down to 1.34 mg/L. While, in stage-2, the sorption system number 1 reduced the concentration from 47.5 to 1.34 mg/L. The volume was varied between 20 mL and 500 mL to observe its effect on optimum adsorbent mass. By substituting equation (2) into equation (9), the material balance as a function of Langmuir constants at each stage can be rewritten as

$$\frac{m_1}{V} = \frac{(C_0-C_1)(1+K_L C_1)}{q_m K_L C_1} \quad (11)$$

$$\frac{m_2}{V} = \frac{(C_1-C_2)(1+K_L C_2)}{q_m K_L C_2} \quad (12)$$

$$\frac{m_1+m_2}{V} = \frac{1}{q_m K_L}\left(\frac{(C_0-C_1)(1+K_L C_1)}{C_1} + \frac{(C_1-C_2)(1+K_L C_2)}{C_2}\right) \quad (13)$$

Equation (13) was differentiated against C_1, where $\frac{\mathrm{d}(m_1+m_2)/V}{\mathrm{d}C_1} = 0$ to yield

$$C_1 = (C_0 C_2)^{\frac{1}{2}} \quad (14)$$

The optimum mass for each stage can be computed by equations (13) and (14). Different removal rates (80 to 99 %) and final concentrations (0.5 to 10 mg/L) in the effluent were set to allow the performance evaluation of the two-stage adsorber. The removal percentage R was calculated by the following equation:

$$R = 100\left(\frac{C_o - C_2}{C_o}\right) \quad (15)$$

Figure 2 illustrates the overall flow of the study.

RESULTS AND DISCUSSION

Adsorption studies

Dye concentration plays a crucial role in the adsorption process. Figure 3 shows the equilibrium adsorption of methylene blue onto adsorbents. The adsorption capacity increased with dye concentration up to a point where maximum removal was achieved. At the point of surface saturation, any further increase in dye concentration may lead to a decline in removal efficiency. At low concentrations, the adsorption capacity was relatively low due to the limited number of dye molecules with respect to the active sites, indicating that the removal process is highly dependent on dye concentration. At high concentrations, the increased driving force helped to overcome mass transfer resistance and enhanced the interaction probabilities of the dye molecules with the adsorbent surface.

CZ1.5 showed a steeper adsorption gradient at low concentrations compared to other adsorbents, indicating a favorable removal of methylene blue. As the concentration increased, the removal of methylene blue by CZ1.5 began to level off at 191 mg/g, whereas CS0.5Z continued to show an upward trend, reaching a Langmuir capacity of 193 mg/g. Generally, the increase in dye removal is attributed to the higher surface area of the adsorbent, which provides more accessible adsorption sites for dye molecule uptake. During activation, dehydration of H_2SO_4 promotes the formation of internal pores by gasifying and combusting the carbon content of the precursor [21].



Figure 2. Overall flow of the study.

In addition, the second activation by $ZnCl_2$ at 600 °C provides adequate heat to release volatile matter and gas, thus causing the formation of more pores [22, 23]. Consequently, the double heating of CS0.5Z likely results in greater porosity, surface area, and adsorption capacity compared to the single-step treatment of CZ1.5. Also, the abundance of surface functional groups on the adsorbent surface enhances the adsorption capacity through several mechanisms, including electrostatic interactions, hydrogen bonding, π-π interactions, and hydrophobic interactions [24, 25]. However, CC exhibits the lowest adsorption capacity, probably due to its non-porous structure and low surface area.

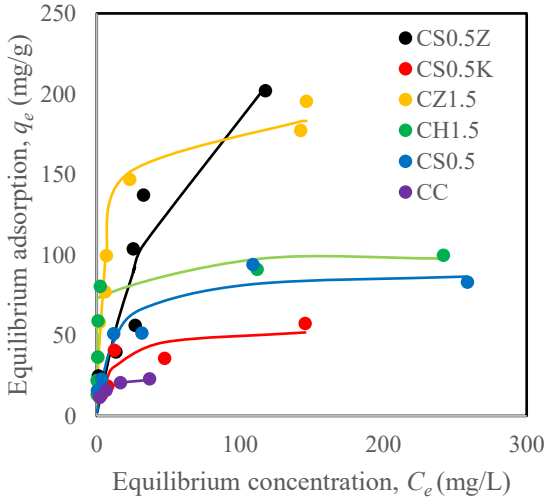

Figure 3 Adsorption of methylene blue onto adsorbents (Lines were predicted by Langmuir model).

The equilibrium distribution of dye molecules between the solid and liquid phases is described by an adsorption isotherm. Table 1 summarizes the isotherm constants for methylene blue adsorption onto adsorbents. The equilibrium data obeyed the Langmuir model with $R^2 > 0.891$, suggesting a single-layer coverage of dye molecules onto a homogeneous surface. An ideal adsorbent should possess both high maximum adsorption capacity and strong affinity K_L [26]. In this work, the affinity shows the favourable removal of methylene blue at low dye concentration, since there are more available binding sites on the adsorbent's surface relative to the amount of dye. The Redlich-Peterson model is a hybrid isotherm that incorporates characteristics of both the Langmuir and Freundlich models. The β values are close to 1, indicating that the Redlich-Peterson isotherm closely resembles the Langmuir isotherm.

Table 1. Isotherm constants for methylene blue adsorption onto adsorbents.

Adsorbent	CS0.5	CS0.5Z	CS0.5K	CZ1.5	CH1.5	CC
Q_{ex} (mg/g)	93.9	202	57.4	195	97.8	22.3
Langmuir						
Q_m (mg/g)	90.4	193	62.9	191	98.1	23.9
K_L (L/mg)	0.0880	0.0155	0.0903	0.168	1.28	0.390
SSE	602	3269	112	961	398	2.74
R^2	0.904	0.891	0.914	0.980	0.947	0.967
Freundlich						
K_f (mg/g) (L/mg)$^{1/n}$	24.0	15.0	13.4	49.0	45.0	10.2
n	4.07	1.82	3.37	3.61	6.55	4.29
SSE	601	3349	230	2260	1910	2.06
R^2	0.879	0.881	0.821	0.941	0.733	0.974
Redlich-Peterson						
K_R	15.7	95241	5.58	56.8	98.4	19.7
α	0.339	6360	0.0892	0.540	0.768	1.39
β	0.877	0.451	0.999	0.879	1.06	0.855
SSE	553	3349	112	579	326	0.719
R^2	0.899	0.881	0.913	0.984	0.954	0.991

Figure 4 shows the adsorption rate of methylene blue onto adsorbents at concentrations of 7.89 and 27.5 mg/L. CZ1.5 and CH1.5 exhibit a faster adsorption rate than CS0.5 and CS0.5Z, resulting in complete dye molecule adsorption more quickly. The transfer of dye molecules from the bulk solution to the boundary layer generally occurs rapidly, whereas their diffusion into the internal pores proceeds at a slower rate [27]. Thus, the larger pore size accounts for the faster adsorption rate by lowering mass transfer resistance and enabling dye molecules to reach active sites more rapidly [28]. Conversely, the slower adsorption rate may be due to the microporous structure of the adsorbent, which can partially restrict the diffusion of dye molecules into the pores [29]. The adsorption rate declined over time, as adsorption sites became progressively occupied, and the adsorbed dye layer induced electrostatic repulsion against the remaining dye molecules in the bulk solution. The decreased adsorption capacity of CS0.5 at 10 mg/L suggests dye molecule desorption, likely caused by weak binding energy with the solid surface. Generally, increasing the dye concentration results in a higher dye removal rate and requires a longer contact time to reach equilibrium. At high dye concentrations, the limited availability of adsorption sites restricts the adsorption process, causing the adsorption rate to decline gradually until it approaches zero.

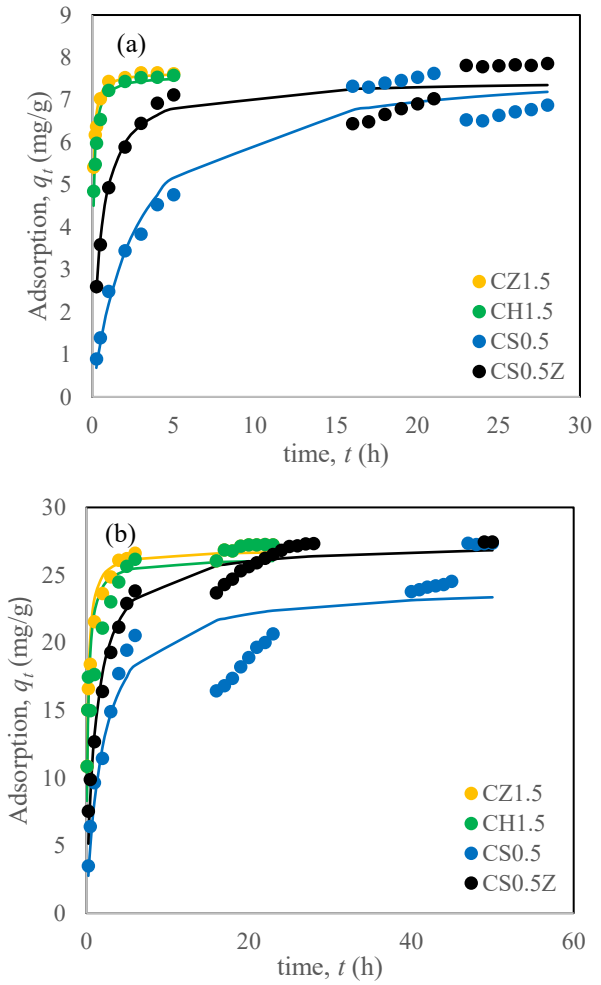

Figure 4. Rate of methylene blue adsorption at (a) 7.89 and (b) 27.5 mg/L onto adsorbents (lines were predicted by a pseudo-second order model).

Table 2 shows the kinetic constants for methylene blue adsorption onto adsorbents. The pseudo-second order model exhibits a higher R^2 value compared to the pseudo-first order model, indicating the applicability of the pseudo-second-order to describe the kinetic data. This suggests that the adsorption is governed by chemical adsorption, involving electron sharing or exchange between the dye molecules and the adsorbent surface [30]. Also, the calculated equilibrium adsorption capacities Q_e closely match the experimental values Q_{ex}, representing good model accuracy. Although the pseudo-second order model provided the best correlation with the experimental data, this alone is not sufficient to conclusively confirm a chemisorption mechanism; therefore, the results were interpreted in terms of adsorption kinetics and possible adsorbate-adsorbent interactions rather than a definitive mechanistic assignment. CZ1.5 exhibits the fastest rate, as reflected by its highest rate constant k_2, values. The increased dye concentration leads to a reduced k_2, thereby extending the time required to attain equilibrium. Nonetheless, the intraparticle diffusion rate constant k_d and C increased at higher dye concentration. The high k_d suggests that dye molecules diffuse into the adsorbent pores more rapidly through pore diffusion than through film diffusion. The high C indicates the increased adsorption rate and boundary layer thickness [16]. In this work, the Q_t *versus* $t^{1/2}$ plot did not pass through the origin, implying that intraparticle diffusion alone does not control the rate and that film diffusion may also be involved [31].

Table 2. Kinetic constants for methylene blue adsorption onto adsorbents.

Adsorbent	CS0.5		CS0.5Z		CZ1.5		CH1.5	
C_o (mg/L)	7.89	27.5	7.89	27.5	7.89	27.5	7.89	27.5
Q_{ex} (mg/g)	6.87	27.4	7.86	27.5	7.63	27.3	7.58	27.3
Pseudo-first order								
Q_e (mg/g)	7.04	22.3	7.17	25.9	7.36	26.0	7.23	25.1
k_1 (h^{-1})	0.289	0.417	1.24	0.557	13.3	4.19	9.98	4.05
SSE	3.63	266	5.40	66.8	1.27	66.1	1.93	170
R^2	0.964	0.743	0.867	0.941	0.773	0.866	0.796	0.679
Pseudo-second order								
Q_e (mg/g)	7.86	24.3	7.48	27.4	7.65	26.9	7.58	26.3
k_2 (g/mg.h)	0.0487	0.0212	0.264	0.0337	3.41	0.239	2.33	0.212
SSE	3.68	197	3.75	23.4	0.126	15.1	0.285	78.4
R^2	0.958	0.808	0.901	0.972	0.976	0.967	0.967	0.846
Intraparticle diffusion								
k_d (mg/g.h)	1.19	2.61	0.705	2.73	0.947	2.43	1.25	2.79
C	1.47	7.98	4.13	12.6	5.90	17.2	5.25	15.5
SSE	11.7	165	11.7	165	1.42	137	1.80	98.1
R^2	0.865	0.838	0.693	0.780	0.728	0.683	0.786	0.798

Characteristics of CZ1.5

Figure 5 shows the characteristics of CZ1.5. The N_2 adsorption-desorption profile exhibits a typical Type IV isotherm with H4 hysteresis, showing the volume adsorbed of 250 mmol/g at relative pressure → 1. The sample endows a surface area of 480 m^2/g with 72% mesopore content and average pore width of 2.91 nm, that is linked to the dehydrating effect of zinc chloride. The SEM image of CZ1.5 displays a rough and irregular surface with interconnected pores ranging from 1 to 10 μm. This implies a transition to mesoporous network with enhanced adsorptive potential for diffusion and surface interaction with dye molecules.

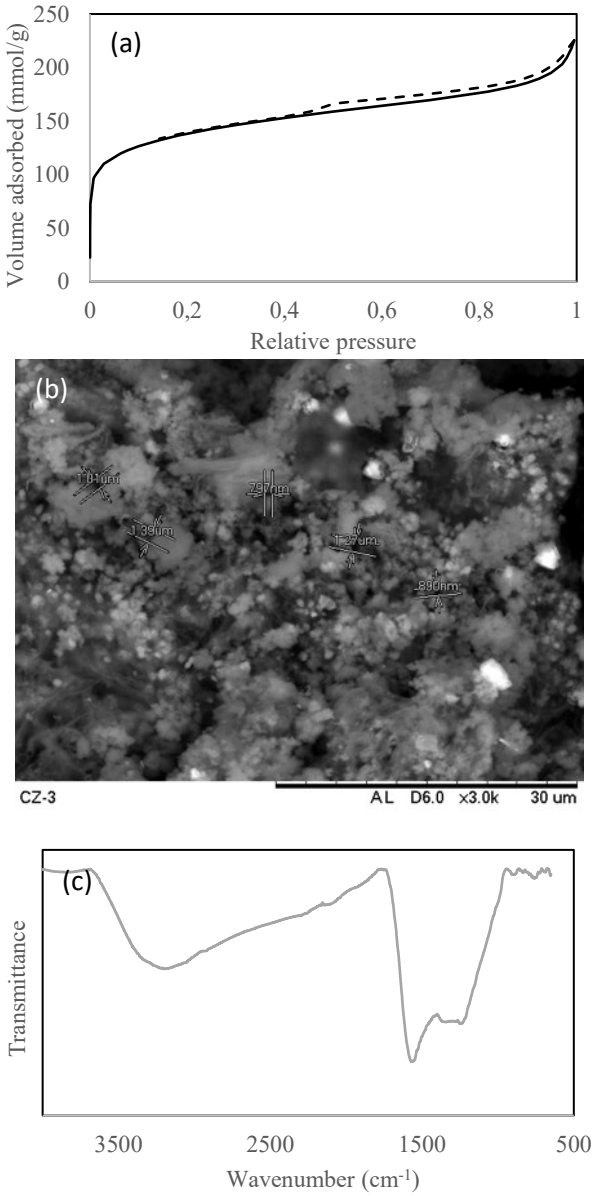

Figure 5. (a) N_2 adsorption-desorption profile (solid line: adsorption branch; dashed line: desorption branch), (b) SEM image and (c) FTIR spectrum of CZ1.5.

The FTIR spectrum shows a broad absorption band at 3500 cm^{-1} that represents O–H stretching vibrations of hydroxyl groups and physisorbed moisture. The peaks in the range of 3000 and 2800 cm^{-1} belong to C–H stretching vibrations of aliphatic hydrocarbon chains. A strong absorption band near 1700 cm^{-1} is attributed to C=O stretching vibrations, signifying the presence of carbonyl groups in CZ1.5. The presence of oxygenated functional groups, such as carboxylic and phenolic groups, at the edges of the carbon matrix is likely to enhance the removal of cationic molecules through electrostatic attraction, ion-exchange and surface complexation. The acidic functionalities increase the density of negatively charged active sites on the adsorbent surface, thereby promoting interactions and improving the adsorption performance.

Two-stage adsorber design

A two-stage adsorber design based on the Langmuir model was proposed for CZ1.5 to reduce the adsorbent mass needed for methylene blue removal. Figure 6(a) shows the profiles of adsorbent mass at different effluent volumes in a two-stage adsorber. The optimum mass of CZ1.5 increases as the volume of dye solution increases to meet 97.3 % removal of methylene blue. As the solution volume increases from 20 to 500 mL, the optimum mass of adsorbent increases from 0.012 to 0.292 g. The optimum mass is estimated at sorption number 18 for all effluent volumes. As the effluent volume increases, the mass gap between the one-stage adsorber (sorption system 1) and the two-stage adsorber (sorption system 18) becomes increasingly pronounced. Consequently, the adsorbent mass can be reduced by 54.8 % at all effluent volumes.

Figure 6(b) shows the mass profiles in each stage of the two-stage batch adsorber to treat 100 mL of methylene blue. In sorption system 18, stage-1 uses 0.042 g of mass, which is higher than the 0.016 g used in stage-2. Stage-1 bears the higher amount of adsorbent because of the high concentration gradient requirement to overcome mass transfer resistance, thereby reducing the amount of adsorbent needed in stage-2 [32].

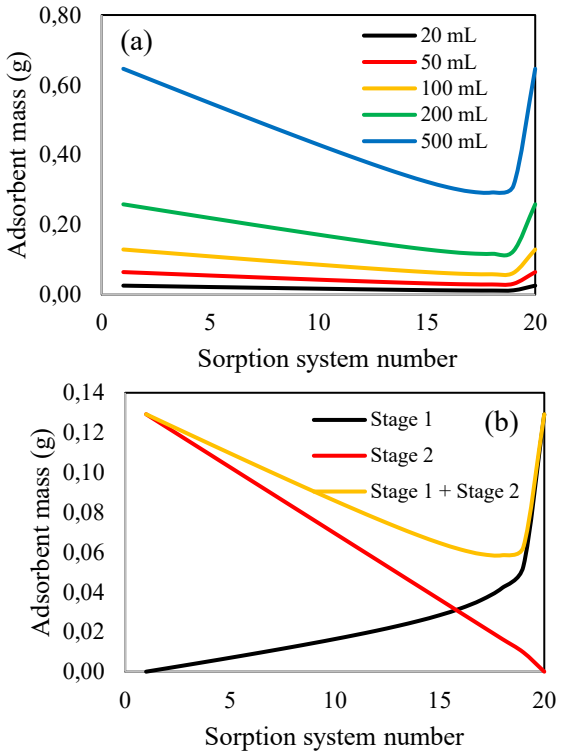

Figure 6. Profiles of adsorbent mass at (a) different effluent volumes and (b) each stage of a two-stage adsorber.

Figure 7 shows the effect of initial concentration C_o on intermediate concentration C_1 at different removal percentages and equilibrium concentrations C_2. From Figure 7(a), C_1 increased with rising C_o, however, as the removal percentage increases, C_1 decreases, indicating increased adsorption capacity. For 80 % removal, initial concentration of 50 mg/L decreased to $C_1 = 22.4$ mg/L, while achieving 99 % removal required a further reduction to $C_1 = 5$ mg/L. Similarly, C_1 is lower when $C_2 = 0.5$ mg/L and the value increases as C_2 increases. The lower C_1 signifies that larger adsorbent mass is applied in stage-1 to substantially decrease the dye concentration, allowing stage-2 to remove the remaining dye concentration at a lower equilibrium.

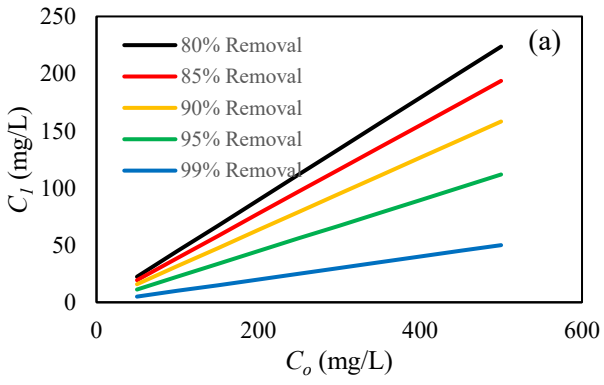

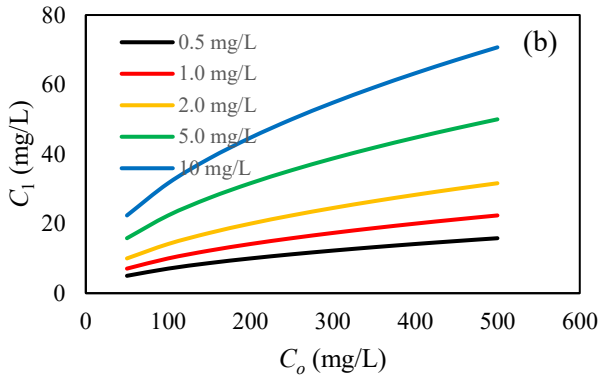

Figure 7. Effect of initial concentration C_o on intermediate concentration C_1 at different (a) removal percentages and (b) equilibrium concentrations C_2.

Figure 8 shows the effects of initial concentration C_o on the total adsorbent mass at different removal percentages and equilibrium concentrations C_2 in a two-stage adsorber. The total mass of adsorbent linearly increases with C_o for all dye removal as shown in Figure 8(a). It means that a larger amount of adsorbent is needed at higher initial concentration and removal percentage. The higher removal efficiency requires larger adsorbent mass to provide sufficient active sites for adsorbent-dye molecule interactions. At C_o = 50 mg/L, the total mass increased from 0.032 g for 80 % removal to 0.555 g for 99 % removal of methylene blue, yielding up to 94.2 % increase in total mass. Thus, the significant increase may be attributed to the weak affinity of the adsorbent surface towards methylene blue molecules [20,33]. The huge leap from 95 to 99 % removal suggests a pronounced effect of liquid-phase mass transfer resistance, which demands a considerably higher quantity of adsorbent to achieve complete dye removal. Likewise, Figure 8(b) shows that a lower C_2 requires more adsorbent mass.

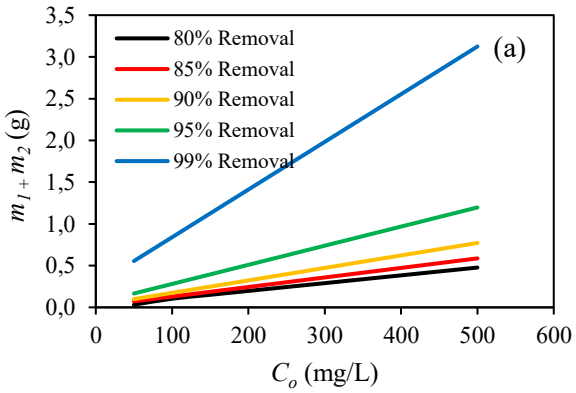

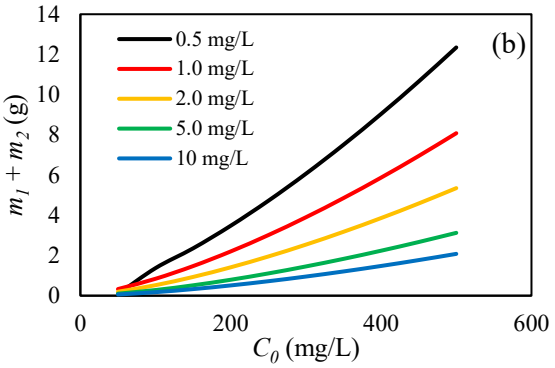

Figure 8. Effect of initial concentration C_o on total mass at different (a) removal percentages, (b) equilibrium concentrations C_2.

Figure 9(a) shows the efficiency of methylene blue removal at both stages for different removal percentages. For every targeted removal performance, the dye removal efficiency in stage-2 (C_1-C_2/m_2) is lower than that in stage-1 (C_o-C_1/m_2). This is due to the reduced dye concentration leaving stage-1 and entering stage-2. Figure 9(b) shows the efficiency of methylene blue removal at stage-2 for different equilibrium concentrations, C_2. Stage-2 efficiency increased with C_2, indicating a more substantial contribution to the overall performance of the two-stage system at elevated target C_2 values.

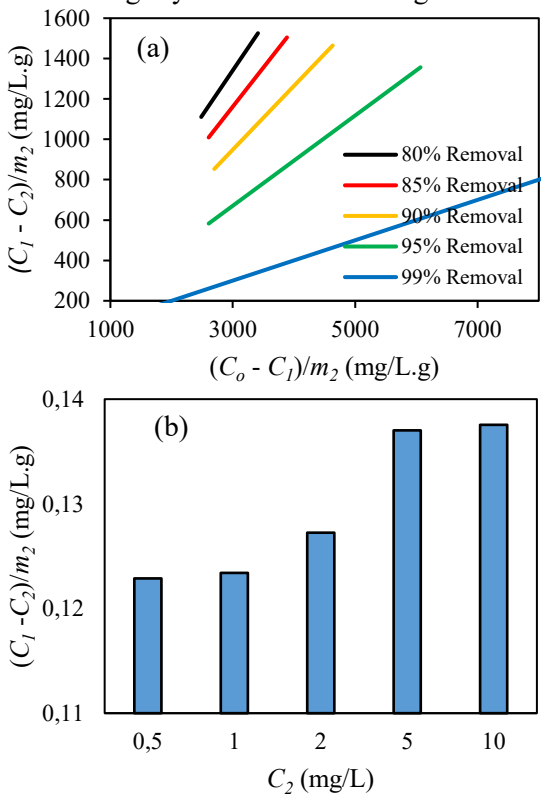

Figure 9. Methylene blue removal at (a) both stages for different removal percentages, and (b) stage-2 for different equilibrium concentrations C_2.

The proposed two-stage adsorber design was developed as a process-scale extension based on experimentally determined Langmuir constants obtained in this study. Although direct experimental validation is not included, the design itself is grounded on an established adsorption model and stage-wise mass balance calculations for preliminary adsorber design.

CONCLUSION

Palm oil condensate was converted into adsorbents *via* chemical activation for methylene blue removal. The removal efficiencies of adsorbents are in the order of CZ1.5 ≈ CS0.5Z > CH1.5 > CS0.5 > CS0.5K > CC. The activation of condensate using H_2SO_4 followed by $ZnCl_2$ activation may results in greater porosity and surface area. Nonetheless, its performance is comparable to the single-step treatment of CZ1.5. In a two-stage adsorber, the mass of CZ1.5 can be minimized to 54.8 % at any volumes, signifying the favorability of oil condensate as carbon feedstock for methylene blue removal. Thus, the two-stage adsorber enhances overall removal efficiency by optimizing carbon mass and lowering process costs.

Acknowledgement/Funding: *This work was supported by the Land and Survey Department of Sarawak through Kursi Premier Sarawak Grant No. 1R037.*

Data availability: *Data will be made available upon request.*

Ethical approval: *Not applicable.*

Competing interests: *All authors declare that they have no competing interests.*

REFERENCES

1. R. V. Khandare, S. P. Govindwar, *Biotechnol. Adv.*, **33** (8), 1697 (2015). http://dx.doi.org/10.1016/j.biotechadv.2015.09.003.
2. M. A. Hassaan, A. E. Nemr, *Am. J. Environ. Sci. Eng.*, **1** (3), 64 (2017). DOI:10.11648/j.ajese.20170103.11.
3. B. M. Adesanmi, Y. -T, Hung, H. H. Paul, C. R. Huhnke, *GSC Adv. Res. Rev.*, **10** (2), 126 (2022). https://doi.org/10.30574/gscarr.2022.10.2.0054.
4. Z. Liu, T. A. Khan, M. A. Islam, U. Tabrez, *Bioresour. Technol.*, **354**, 127168 (2022). https://doi.org/10.1016/j.biortech.2022.127168.
5. Y. Liu, J. Chen, D. Duan, Z. Zhang, C. Liu, W. Cai, Z. Zhao, *Sustainability*, **16**, 10867 (2024). https://doi.org/10.3390/su162410867.
6. Y. Song, L. Wang, X. Qiang, W. Gu, Z. Ma, G. Wang, *J. Water Process. Eng.*, **55**, 104242 (2023). https://doi.org/10.1016/j.jwpe.2023.104242.
7. F. Mbarki, T. Selmi, A. Kesraoui, M. Seffen, *Ind. Crops Prod.*, **178**, 114546 (2022). 10.1016/j.indcrop.2022.114546.

8. D. B. Pal, A. Singh, J. M. Jha, N. Srivastava, A. Hashem, M. A. Alakeel, E. F. Abd_Allah, V. K. Gupta, *Bioresour. Technol*., **339**, 125606 (2021). https://doi.org/10.1016/j.biortech.2021.125606.
9. S. Hamdi, A. Miguez-Gonzalez, R. Cela-Dablanca, A. Barreiro, M. J. Fernandez-Sanjurjo, A. Nunez-Delgado, E. Álvarez-Rodriguez, *J. Environ. Manage*., **368**, 122158 (2024). https://doi.org/10.1016/ j. jenvman.2024.122158.
10. L. Velarde, D. Nikjoo, E. Escalera, F. Akhtar, *Heliyon*, **10** (1), e24006 (2024). https://doi.org/10.1016/j.heliyon.2024.e24006.
11. J. Saleem, Z. K. B. Moghal, S. Pradhan, G. McKay, *RSC Adv*., **14** (46), 33797 (2024). doi: 10.1039/d4ra06287f.
12. M. Moheb, A. M. El-Wakila, F. S. Awad, *RSC Adv*., **15**, 674 (2025). DOI: 10.1039/D4RA07957D.
13. X. Zhang, L. Cheng, X. Wu, Y. Tang, Y. Wu, *J. Environ. Sci*., **33**, 97 (2015). https://doi.org/10.1016/j. jes.2015.01.014.
14. A. K. M. Omar, T. L. T. Norsalwani, M. S. Asmah, Z. Y. Badrulhisham, A. M. Easa, F. M. Omar, M. S. Hossain, M. H. Zuknik, N. A. N. Norulaini, *J. CO_2 Util.,* **25**, 205 (2018). https://doi.org/10.1016/j. jcou.2018.03.021.
15. G. K. A. Parveez, S. -S. Leow, N. N. Kamil, A. Z. Madihah, M. Ithnin, M. H. Ng, Y. A. Yusof, Z. Idris, *J. Oil Palm Res*., **36** (2), 171 (2024). https://doi.org/10.21894/jopr.2024.0037.
16. F. Amran, M. A. A. Zaini, *Surf. Interfaces,* **25**, 101277 (2021). https://doi.org/10.1016/j.surfin. 2021.101277F.
17. H. Palanisami, M. R. M. Azmi, M. A. A. Zaini, Z. A. Zakaria, M. N. H. Z. Alam, M. A. C. Yunus, *Water Pract. Technol*., **16** (3), 793 (2021). https://doi.org/10.2166/wpt.2021.034.
18. M. Hijab, P. Parthasarathy, H. R. Mackey, T. Al-Ansari, G. McKay, *Chem. Eng. Process: Process Intensif*., **167**, 108318 (2021). https://doi.org/10.1016/j.cep.2021.108318.
19. M. A. K. Anuar, N. Mahat, N. M. Rusli, M. N. H. Z. Alam, M. A. A. Zaini, *Int. J. Biomass Renew*., **10** (2), 1 (2021). DOI:10.61762/ijbrvol10iss2art12871.
20. S. A. H. Azaman, A. Afandi, B. H. Hameed, A. T. M. Din, *J. Appl. Sci. Eng*., **21** (3), 317 (2018). DOI:10.6180/jase.201809_21(3).0003.
21. N. Samghouli, I. Bencheikh, K. Azoulay, S. Jansson, S. E. Hajjaji, *Environ. Monit. Assess*., **197**, 259 (2025). https://doi.org/10.1007/s10661-025-13685-4.
22. P. E. Hock, M. A. A. Zaini, *Acta Chim. Slovaca*, **11** (2), 99 (2018). DOI: 10.2478/acs-2018-0015.
23. B. Li, J. Hu, H. Xiong, Y. Xiao, *ACS Omega*, **5**, 9398 (2020). https://dx.doi.org/10.1021/acsomega.0c00461.
24. T. K. Bui, L. T. Nguyen, T. M. Cao, V. V. Pham, *ACS Symp. Ser*., **1478**, 1 (2024). DOI: 10.1021/bk-2024-1478.ch001.
25. K. H. H. Aziz, N. M. Fatah, K. T. Muhammad, *R. Soc. Open Sci*., **11**, 232033 (2024). https://doi.org/10.1098/rsos.232033.
26. A. D. Sponza, N. J. Fernandez, D. Yang, K. A. Ortiz, A. E. Navarro, *Environments*, **2**, 388 (2015). DOI:10.3390/environments2030388.
27. B. An, *Processes*, **8**, 1194 (2020). DOI:10.3390/pr8091194.
28. S. Chen, X. Wang, W. Tong, J. Sun, X. Xu, J. Song, J. Gong, W. Chen, *Nanomaterials*, **11** (3), 799 (2021). https://doi.org/10.3390/nano11030799.
29. M. S. Musa, I. Rosazhar, F Amran, M. A. A. Zaini, *Chem. Afr*., **7**, 5577 (2024). https://doi.org/10.1007/s42250-024-01124-9.
30. M. I. Khan, S. Sufian, F. Hassan, R. Shamsuddin, M. Farooq, *RSC Adv*., **15**, 1989 (2025). https://doi.org/10.1039/D4RA05782A.
31. S. M. Nasser, M. Abbas, M. Trari, *Prog. React. Kinet. Mech*., **49**, 1 (2024). https://doi.org/10.1177/14686783241226858.
32. T. Sarawanan, N. Mahat, N. M. Rusli, M. A. A. Zaini, *Chem. Prod. Process Model*., **18** (3), 1 (2022). https://doi.org/10.1515/cppm-2022-0010.
33. Amran, N. F. Zainuddin, M. A. A. Zaini, *Malays. J. Fundam. Appl. Sci.,* 17**,** 768 (2021). DOI:10.11113/mjfas.v17n6.2303.